



# Impedance-based structural health monitoring applied to steel fiber-reinforced concrete structures

R. N. Fernandes Silva<sup>1</sup> · K. M. Tsuruta<sup>2</sup> · D. S. Rabelo<sup>3</sup> · R. M. Finzi Neto<sup>2</sup> · A. A. Cavalini Jr.<sup>2</sup> · V. Steffen Jr.<sup>2</sup>

Received: 27 September 2019 / Accepted: 12 June 2020 / Published online: 30 June 2020  
© The Brazilian Society of Mechanical Sciences and Engineering 2020

## Abstract

The goal of the present contribution is to test the effectiveness of an impedance-based structural health monitoring (ISHM) methodology to detect damage in steel fiber-reinforced concrete structures. For this aim, a piezoceramic sensor coated with epoxy is used. A prismatic concrete specimen was evaluated for the case in which the damage condition was obtained from compression testing. The impedance signatures were measured both before and after the compression testing for the specimens placed inside an environmental chamber. An optimization procedure was applied to compensate for the temperature effects that appear on the impedance signatures. For illustration purposes, the coated piezoelectric transducer was initially bonded to the surface of an aluminum beam to detect damage induced by a loosening bolt. An impedance analyzer was used to measure impedance signatures in the frequency range of 40–70 kHz for the procedure with the aluminum beam and 50–80 kHz for the prismatic steel fiber concrete specimen. An in-house portable impedance meter (SySHM impedance meter) was used to measure the impedance signatures. The results encourage the use of the ISHM approach for health monitoring of steel fiber-reinforced concrete structures.

**Keywords** Steel fiber-reinforced concrete structures · Impedance-based structural health monitoring (ISHM) · Temperature compensation · Optimization · Piezoceramic sensor

## 1 Introduction

Failure in civil engineering structures can lead to considerable economic losses. Therefore, many researchers have been developing real-time nondestructive techniques to detect incipient damage in steel fiber concrete structures, in order to both improve their safety and increase their useful life. Among various damage detection technologies, structural health monitoring (SHM) provides means to assess a structure in real time, with promising features [1, 2].

The application of SHM techniques to civil engineering structures is not simple to be implemented since there are limitations associated with the size of the structure, the location of possible damages, and the cost associated with the sensor array and signal processing [3]. The literature brings several contributions on SHM techniques developed for concrete structures that are based on vibration responses [4, 5], optical fiber [6, 7], and the electromechanical impedance approach [8–10]. The methods based on vibration data normally use low frequencies in the analyses, and only major damage can be detected [11]. The technique based on optical fibers presents some disadvantages since the concrete is brittle and heterogeneous (several sizes of aggregates). At a low level of load, the structure cracks and may lead to a break and debonding of the optical fiber [7]. It is worth mentioning that the impedance-based structural health monitoring technique (ISHM) that is tested in the present contribution is showing promising results [8–10]. It is observed that this technique is widely applied to several types of structures; however, this methodology has also some disadvantages such as the influence of temperature on the impedance signals [11].

Technical Editor: Pedro Manuel Calas Lopes Pacheco, D.Sc.

✉ R. N. Fernandes Silva  
raquelfernandes@ufu.br

<sup>1</sup> School of Civil Engineering, Federal University of Uberlândia, Uberlândia, Brazil

<sup>2</sup> School of Mechanical Engineering, Federal University of Uberlândia, Uberlândia, Brazil

<sup>3</sup> Faculty of Sciences and Technology, Federal University of Goiás, Aparecida de Goiânia, Brazil

The ISHM technique uses piezoelectric transducers that are bonded on the surface of the structure or embedded into it. As a smart material, a piezoelectric transducer works simultaneously as sensor (inverse piezoelectric effect) and actuator (direct piezoelectric effect). This technique has been successfully applied to a wide variety of structures and conditions, as reported in the literature. The basic concept of ISHM is to look for modifications on the mechanical impedance signatures of the monitored structure under the existence of damage. However, measuring the mechanical impedance directly on the structure is not an easy task. Instead, measurements of variations in the mechanical impedance are performed by measuring the electrical impedance from piezoelectric transducers [typically composed with lead zirconate titanate (PZT)] coupled to the host structure. Due to the electromechanical coupling between the PZT transducers and the structure, the existence of damage in the structure can be perceived from the change between a baseline signature and the current test signature. This change is a result of modifications on the dynamic properties of the structure as caused by damage [12].

One of the first published reports on this subject for civil structures showed that the electromechanical impedance method was successful for crack detection in the context of loading and unloading a prototype formed by a part of a bridge of reinforced concrete [13]. Other studies have also obtained promising results such as, for instance, on detecting damage in concrete plates where the damage was produced by a cutting blade [14, 15]. In [16], the authors analyzed the influence of the concrete cure on the impedance signals. For this aim, a piezoelectric transducer was embedded into the concrete plate during its manufacturing stage. It was found that the impedance signals change as the samples were subjected to compression. However, the authors did not conduct more detailed studies regarding the existence of incipient damage. A study about the influence of sensor debonding on impedance signatures was performed in [17]. In this case, the sensors were bonded to the steel fibers used to reinforce concrete structures. In [18] the ISHM technique was conducted to detect carbonation in concrete structures.

Other studies evaluated the adhesive based on epoxy resins; Lim et al. [19] analyzed the feasibility of the use of ISHM and piezoelectric wave velocity methods to monitor the cure of the structural adhesive using piezoelectric transducers; in addition, [20] used an analytical and numerical modeling based on finite elements for piezoelectric wave technique to monitor curing process of structural adhesives. Besides, Gupta et al. [21] proposed a noncontact and non-intrusive imaging technique to monitor the curing of epoxy resins; for this aim, an electrical capacitance tomography was employed to characterize changes in the distribution of electrical permittivity of epoxy specimens during curing process.

As previously mentioned, the piezoelectric transducers used by the ISHM approach are brittle, which justifies the development of a protective coat for the sensors [16, 22–25]. Thus, it is possible to embed the sensors into civil structures. A simple method was presented by [20] to incorporate the PZT transducer into the concrete structure. The protection of the sensors was provided by a wire mesh of steel and cement paste [22]. The influence of temperature and the loading on impedance signals using a piezoelectric transducer coated with cement and epoxy resin was studied by [24]. The authors of Liu et al. [25] proposed a method to monitor freezing–thawing and crack damage in concrete using PZT transducers packaged with cement, epoxy resin and a hardener.

Finally, the impedance-based monitoring techniques have also been employed in different damage detection applications, including corrosion [26], severity of debonding [27], weak bond detection [28], and interfacial debonding [29]. Apart from damage detection and strength gain monitoring, the impedance-based monitoring techniques are also employed to detect the changes in structural stress [30, 31].

However, there is a clear need for refining the ISHM technique with respect to its application on concrete structures. The main contribution of this paper is to evaluate the ISHM technique using the piezoelectric transducer coated with epoxy as a sensor and actuator embedded in a concrete specimen to detect damage during structural damage progression. In addition, the behavior of the impedance signature is analyzed for the scenario in which temperature is changing. Consequently, by analyzing the results obtained in the present study, it is possible to demonstrate that incipient cracks can be reliably detected with the ISHM method in association with a data normalization technique for temperature compensation. In this context, the objective of the present work is to test the effectiveness of a piezoelectric transducer protected by an epoxy coating to detect damage in civil engineering structures by using the ISHM approach. In addition, an optimization method was implemented to compensate for the temperature variation on the impedance signatures.

## 2 Electromechanical impedance method: a review

The ISHM technique uses piezoelectric transducers coupled to the host structure. By using their sensor and actuator properties to detect damage, these transducers monitor changes on the stiffness, damping, and mass of the structure. The coupling to the structure permits the use of the electromechanical coupling characteristics of piezoelectric transducers. For this aim, an electrical impedance measurement is acquired from the piezoelectric transducers due to

the difficulty in obtaining the mechanical impedance of the structure, directly. Typically, PZT (lead zirconate titanate) transducers are used. Considering that the properties of the PZT transducer do not vary over time, changes in the electrical impedance will be directly related to changes in the mechanical impedance, which is affected by the presence of damage [12].

Figure 1 shows a single-degree-of-freedom (DOF) electromechanical model that describes the measurement process of the impedance signal [12]. The piezoelectric transducer is bonded directly to the structure surface by using a high-strength adhesive to ensure high electromechanical coupling [13]. The dynamic properties of the monitored structure are represented by the mass  $m$ , stiffness  $k$ , and damping  $c$ . The piezoelectric transducer is excited by a sinusoidal voltage source  $V_i(\omega)$  with amplitude  $V$  and frequency  $\omega$ . Consequently, from the actuator effect, the piezoelectric transducer applies a force on the host structure. The corresponding vibration response of the structure induces a strain on the piezoelectric transducer, which, from the sensor effect, generates an output current  $I_o(\omega)$  with amplitude  $I$ , frequency  $\omega$ , and phase  $\phi$ . The mechanical impedance  $Z_m(\omega)$  of the monitored structure is given by the relation between the applied force  $F(\omega)$  to the structure and its response velocity  $\dot{X}(\omega)$ . However, the measurement of the mechanical impedance is demonstrated to be a difficult task. Making an analogy to an electric circuit, the force and velocity correspond to the voltage and output current, respectively, resulting in the electrical impedance  $Z_e(\omega)$ . The electrical impedance of the PZT transducer can be measured by using an appropriate impedance meter. It is worth mentioning that any deviation on the mechanical properties of the structure (mass  $m$ , stiffness  $k$ , and damping  $c$ ) of the PZT transducer is directly related to changes in the mechanical impedance. Consequently, faults can be detected by measuring the electrical impedance of the PZT transducer.

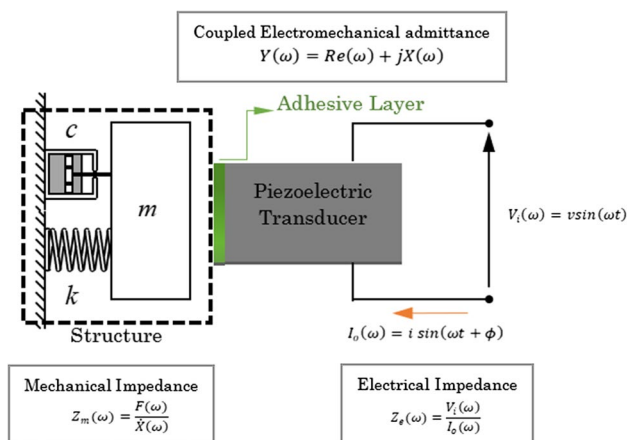


Fig. 1 A single-DOF electromechanical model of the ISHM [12]

It is worth mentioning that the direct piezoelectric effect (or sensor effect) is characterized by producing a voltage when the piezoelectric transducer is mechanically deformed in its elastic phase. The inverse effect (or actuator effect) appears when a piezoceramic transducer is subjected to a voltage, resulting in a mechanical deformation [13].

Equation 1 shows the frequency-dependent electrical admittance, which represents the wave equation of a piezoelectric transducer coupled to the host structure [12]. Based on the system shown by Fig. 1, the admittance  $Y(\omega)$  (inverse of impedance) of the piezoelectric transducer is a combined function involving the mechanical impedance of the PZT actuator  $Z_a(\omega)$  and the structure  $Z_s(\omega)$ :

$$Y(\omega) = R(\omega) + jX(\omega) = \frac{I_o(\omega)}{V_i(\omega)} = j\omega \frac{b_a l_a}{h_a} \left( \epsilon_{33}^{-T} (1 - j\lambda) - \frac{Z_s(\omega)}{Z_s(\omega) + Z_a(\omega)} d_{31}^2 \hat{Y}_{11}^E \right) \quad (1)$$

where  $R(\omega)$  and  $X(\omega)$  are the real part and imaginary part of the electromechanical admittance, respectively,  $j$  is the imaginary unit,  $\omega$  is the angular frequency,  $b_a$ ,  $l_a$ , and  $h_a$  are the width, length, and thickness of the piezoelectric transducer, respectively,  $\epsilon_{33}^T$  is the dielectric constant at zero stress,  $\lambda$  is the dielectric loss tangent to the piezoelectric transducer,  $d_{31}$  is the piezoelectric coupling constant at zero electric field, and  $\hat{Y}_{11}^E$  is the complex Young's modulus of the PZT transducer with zero electric field. The impedance is a frequency-dependent complex function. To obtain the electrical impedance, both the direct and inverse effects of the piezoelectric transducer participate. In the ISHM approach, trial-and-error tests should be previously performed aiming at identifying the most sensitive frequency band with respect to fault presence [13].

In the ISHM method, damages are detected based on the comparison between the real part of the impedance signatures acquired from both the healthy and faulty (or unknown) structure conditions. A visual examination of the signals is not enough for evaluation since it gives only a qualitative comparison. Consequently, it is necessary to use adequate damage metrics for defining quantitative criteria. Thus, damage metrics are employed, which are properly defined scalar parameters, so that they can numerically represent the difference between the two signals (without and with damage) [32]. Several damage metrics have been proposed to compare impedance signatures [33]. For instance, one of the most commonly used is the root-mean-square deviation (RMSD) and its definition is given by Eq. (2) [34, 35]:

$$\text{RMSD} = \left\{ \sum_{i=1}^n \frac{[\text{Re}(Z_{1i}) - \text{Re}(Z_{2i})]^2}{\text{Re}(Z_{1i})^2} \right\}^{1/2} \quad (2)$$

where  $\text{Re}(Z_{1i})$  is the real part of the impedance measure without damage (baseline) at the frequency  $i$ .  $\text{Re}(Z_{2i})$  is the real part of the impedance measurement at the frequency  $i$  for a new (unknown) structural configuration, and  $n$  is the total number of points used in the measurements.

Another important metric found in the literature is the deviation of the correlation coefficient (CCD). This metric is used to quantify and interpret the information contained in datasets. Its mathematical definition involves the difference between a coefficient of correlation between a measurement and a reference value, as given by Eq. (3) [36]:

$$\text{CCD} = 1 - \text{CC} \tag{3}$$

where CCD is the deviation of the correlation coefficient and CC is the correlation coefficient, as calculated by Eq. 4:

$$\text{CC} = \frac{1}{n} \sum_{i=1}^n \frac{[\text{Re}(Z_{1i}) - \text{Re}(\bar{Z}_{1i})] - [\text{Re}(Z_{2i}) - \text{Re}(\bar{Z}_{2i})]}{S_{Z1}S_{Z2}} \tag{4}$$

in which  $S_{Z1}$  is the standard deviation of the baseline impedance signal and  $S_{Z2}$  is the standard deviation of the impedance signal to be compared with. If the correlation coefficient is equal to 1.0, the signals have a full correlation. When the difference between the two signals is higher, the value of CC is smaller. It is worth mentioning that the value of CC is also used to compare and quantify impedance signals.

### 3 Temperature compensation through an optimization procedure

Temperature variation effects are known to change impedance signatures. A review of temperature variation effects and compensation methods can be found in [37, 38]. Figure 2 shows a flowchart to illustrate the proposed temperature compensation approach. The method starts by obtaining the impedance signatures of the healthy system evaluated

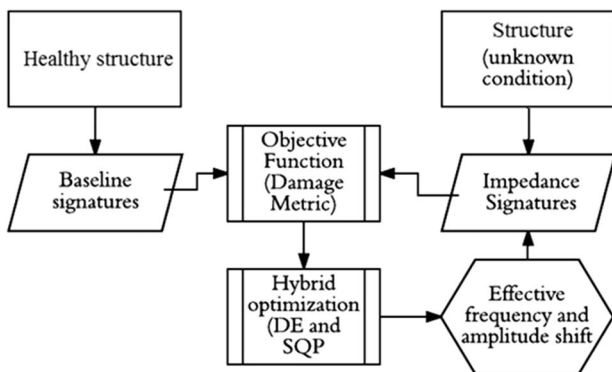


Fig. 2 Proposed temperature compensation flowchart

(impedance:  $Z_1$ ; temperature:  $T_{\text{baseline}}$ ). The impedance signatures of the system for an unknown condition (impedance:  $Z_2$ ; temperature:  $T_{\text{unknown}} \neq T_{\text{baseline}}$ ) are also required, so that the optimizer is responsible for shifting both the frequency and amplitude values. The impedance signature  $Z_2$  is compared with  $Z_1$  by means of a given objective function, i.e., a damage metric, as presented by Eqs. (2) and (3). In Fig. 2, if the procedure converges to a minimum value of the objective function, the effects of temperature variation are compensated through frequency shifts and vertical shifts of the design variables. If this is not the case, the optimization procedure continues the search for new frequency and amplitude shifts. The optimization process continues iteratively until convergence is achieved, which can lead to temperature compensation (if the objective function is close to zero) or, otherwise, represents a damage indication associated with temperature compensation.

In the present contribution, a hybrid optimization technique is primarily devoted to minimizing the influence of temperature variation during the impedance measurement process. In the following, the proposed hybrid optimization algorithm is briefly described. In this sense, the evolutionary technique differential evolution (DE) [39] is devoted to the global search for the optimum (i.e., the effective frequency and amplitude shifts). It is worth mentioning that the DE algorithm must be performed  $m$  times to avoid local minima. The best result obtained by DE is then used as a starting point for the classical direct method known as sequential quadratic programming (SQP) to obtain the local and refined optimal solution.

The DE algorithm is an optimization technique that belongs to the family of evolutionary computation, which differs from other evolutionary algorithms in the mutation and recombination schemes. DE executes its mutation operation by adding a weighted difference vector between two individuals to a third one. Then, the mutated individuals will perform discrete crossover and greedy selection with the corresponding individuals from the last generation to produce the offspring. The key control parameters of DE are the population size (NP), the crossover constant (CR), and the associated weight (FDE).

The pseudocode of DE algorithm is presented in Fig. 3, in which  $P$  is the population of the current generation,  $P'$  is the population to be constructed for the next generation,  $C[i]$  is the candidate solution with population index  $i$ ,  $C[i][j]$  is the  $j$ th entry in the solution vector of  $C[i]$ , and  $r$  is a random number between 0 and 1. In [40], simple rules are given for choosing the key parameters of DE for general applications. Normally, NP should be about 5–10 times the dimension of the problem (i.e., the number of design variables). As for FDE, it lies in the range between 0.4 and 1.0. Initially, FDE=0.5 can be tried, and then FDE and/or NP can be increased if the population converges prematurely. In [41], various mutation schemes have

**Fig. 3** Pseudocode of DE algorithm

```

Differential Evolution
Initialize and evaluate population P
while (not done) {
  for (i = 0; i < N; i++) {
    Create candidate C[i]
    Evaluate C[i]
    if (C[i] is better than P[i])
      P0[i] = C[i]
    else
      P0[i] = P[i]
    P = P0
  }
  Create candidate C[i]
  Randomly select parents P[i1], P[i2], and P[i3]
  where i, i1, i2, and i3 are different.
  Create initial candidate
  C'[i] = P[i1] + F × (P[i2] - P[i3]).
  Create final candidate C[i] by crossing over the genes of P[i] and C'[i] as follows:
  for (j = 0; j < N; j++) {
    if (r < CR)
      C[i][j] = C'[i][j]
    else
      C[i][j] = P[i][j]
  }
}
    
```

been proposed for the generation of new candidate solutions by combining the vectors that are randomly chosen from the current population. In the applications presented in this paper, the rand/1 scheme was used.

According to [41], the SQP algorithm is a direct method used for dealing with constrained minimization problems in which the search direction *S* is found by solving a subproblem with a quadratic objective function and linear constraints. For this purpose, a quadratic approximation of the augmented objective function (i.e., from the association of the Lagrange multipliers  $\lambda$  with an exterior penalty technique) and a linear approximation for constraints are written, as shown in Eq. (5):

$$\begin{aligned}
 \text{Minimize: } & Q(S) = F(X) + \nabla F(X)^T S + \frac{1}{2} S^T B S \\
 \text{Subject to: } & \nabla g_j(X)^T S + \delta_j g_j(X) \leq 0 \quad j = 1, m \\
 & \nabla h_k(X)^T S + \delta h_k(X) \leq 0 \quad k = 1, l
 \end{aligned}
 \tag{5}$$

where *F(X)* is the function to be minimized, *X* is the vector of design variables,  $\nabla F$  is the gradient of *F*, *S* is the search direction vector, and *B* is initially an identity matrix that will be updated on subsequent iterations. The parameters  $\delta_j$  and  $\delta$  are used to prevent inconsistencies between the linearized constraints *g<sub>j</sub>* and *h<sub>k</sub>* (i.e., typically  $0.9 \leq \delta \leq 0.95$ ).  $\nabla g_j$  and  $\nabla h_k$  are the gradients of *g<sub>j</sub>* and *h<sub>k</sub>*, respectively. The parameter  $\delta_j$  is defined as follows:

$$\begin{aligned}
 \delta_j &= 1 \quad \text{if } g_j(X) < 0 \\
 \delta_j &= \bar{\delta} \quad \text{if } g_j(X) \geq 0
 \end{aligned}
 \tag{6}$$

The one-dimensional search, described by Eq. (5), is a quadratic programming problem, and various techniques are available for its solution. The associated one-dimensional search is written from the determined search direction *S* and an exterior penalty function  $\phi$ , as given by Eq. (7):

$$\phi = F(X) + \sum_{j=1}^m u_j \{ \max[0, g_j(X)] \} + \sum_{k=1}^l u_{m+k} |h_k(X)| \tag{7}$$

where  $X = X_{q-1} + \alpha_p S$ ,  $u_j = |\lambda_j|$  ( $j = 1, m + 1$ ) in the first iteration,  $u_j = \max [|\lambda_j|, 0.5 (u'_j + |\lambda_j|)]$  for the subsequent iterations, and  $u'_j = u_j$  from the previous iteration (*q* is the iteration). In this case, the step length parameter is defined as  $\alpha_p = 1$  (i.e., convergence parameter).

### 4 Statistical threshold determination

The concepts behind statistical process control allow for establishing limits in a control chart so that a threshold can be established using the upper control limit [37]. These limits can be defined so that either 95.45% or 99.73% of data from a normally distributed population remain if these control limits are defined as expressed in Eq. (8):

$$\begin{aligned}
 \bar{x} \pm 2s & \quad \text{for } 95.45\% \text{ confidence} \\
 \bar{x} \pm 3s & \quad \text{for } 99.73\% \text{ confidence}
 \end{aligned}
 \tag{8}$$



where  $\bar{x}$  is the sample mean and  $s$  is the sample standard deviation. Each sample  $x$  is determined by using the damage metrics [see Eqs. (2) and (3)].

In the ISHM approach, the upper control limit is used for the threshold determination. Although the expressions in Eq. (8) can provide the threshold calculation, it should be noted that the mean values and standard deviations of the samples are inferences from the population parameters (i.e., unknown values). Therefore, a more robust methodology is proposed by using the upper limits of the confidence intervals for the population mean and standard deviation according to Eqs. (9) and (10), respectively [42]:

$$\bar{x} - \frac{St_{v;\alpha/2}}{\sqrt{N}} \leq \mu_x \leq \bar{x} + \frac{St_{v;\alpha/2}}{\sqrt{N}}; v = N - 1 \quad (9)$$

$$\frac{vs^2}{\chi^2_{v;\alpha/2}} \leq \sigma_x^2 \leq \frac{vs^2}{\chi^2_{v;1-\alpha/2}}; v = N - 1 \quad (10)$$

where  $\mu_x$  and  $\sigma_x^2$  are the population mean and variance, respectively,  $\bar{x}$  and  $s^2$  are the sample mean and variance, respectively,  $t_{v;\alpha/2}$  has a student t distribution with  $v$  DOF,  $\alpha$  is the significance level, and  $\chi^2_{v;\alpha/2}$  follows a Chi-square distribution.

Hence, the upper limit of the confidence intervals was used and the threshold for each PZT transducer was determined through Eq. (11):

$$PZT_{\text{threshold}} = \mu_{x_{\text{max}}} + 3\sigma_{x_{\text{max}}} \quad (11)$$

where  $\mu_{x_{\text{max}}}$  is the upper limit for the population mean and  $\sigma_{x_{\text{max}}}$  is the upper limit for the population standard deviation, both obtained by choosing 5% for the significance level  $\alpha$ .

## 5 Methodology

For the sake of clarity, this section presents experimental applications of the ISHM technique to both an aluminum beam and a sample of prismatic concrete. Initially, it will be shown how the coated piezoceramic was produced. More details can be found in [43].

The first experiment was carried out to observe the functionality of the coated piezoceramic transducer on the aluminum beam. Considering the positive results, it was possible to mold the concrete sample with the embedded coated piezoelectric transducer, in order to evaluate the efficiency of the protection by applying the ISHM technique on the concrete. Here, two different tests were carried out independently. In the first set up experiment, the signals were measured before and after the damage was generated, since it was not possible to introduce the damage inside the thermal

chamber without changing the boundary conditions of the specimen. In the second experiment with this sample, the signals were collected before, during and after the test that generated the damage. In all cases, the frequency range was determined experimentally by analyzing the peak density in this region, which corresponds to a good electromechanical coupling. The literature on this subject suggests that this interval is usually sufficient to detect damage of the magnitude that was tested in this paper [11].

It is worth mentioning that the optimization procedure was applied to compensate for the effects of temperature on the impedance signatures in all experiments. This procedure searches for optimal shifts (in both frequency and amplitude), which minimize the objective function (damage metric). By doing so, the correlation of the signals is maximized, thus promoting the removal of the influence of shifts on the signatures as caused by temperature change.

The process was performed according to the following steps:

- Experimental setup: preparation of specimens and test configurations;
- Impedance measurements;
- Obtain damage metrics and implement optimization procedure;
- Determine statistical thresholds and compute structural diagnostics.

### 5.1 Coated piezoelectric transducer

As the nature of the experiment carried out in this study promotes significant mechanical loading to the analyzed concrete structure, a protective layer was designed in order to ensure that the sensor would remain healthy all along the inherent operational loadings. For this aim, an epoxy resin-based adhesive was used to protect the sensor from possible collapse within the concrete. The coating is a resin with high adhesion capacity for bonding large smooth, porous, and irregular surfaces, such as tiles, wood, glass, concrete, stones, metals, and some rigid plastics, capable of withstanding temperatures up to 80 °C and with greater resistance than concrete ( $\cong 100$  MPa).

Molding the coating requires a curing period of 24 h, with four hours for the first layer on which the piezoelectric sensor is located. At the end of this process, the coated piezoelectric transducer has a final diameter of 40.0 mm, thickness of 4.0 mm, and a mass of approximately 20.0 g (Fig. 4). In this experiment, piezoelectric transducers known as PZT's (lead zirconate titanate) type 5H model were used.

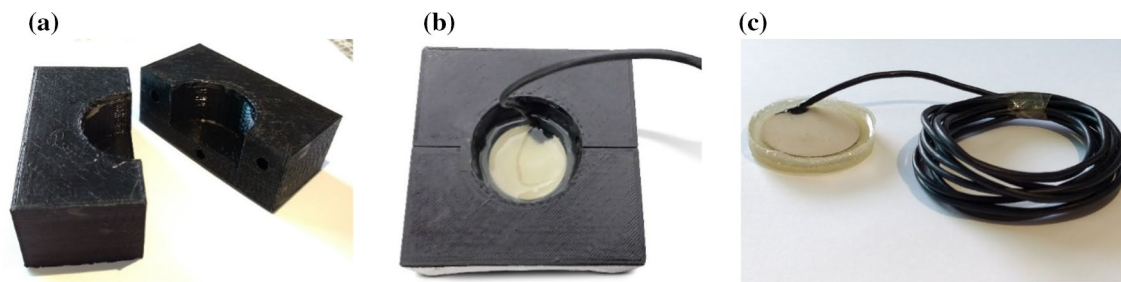
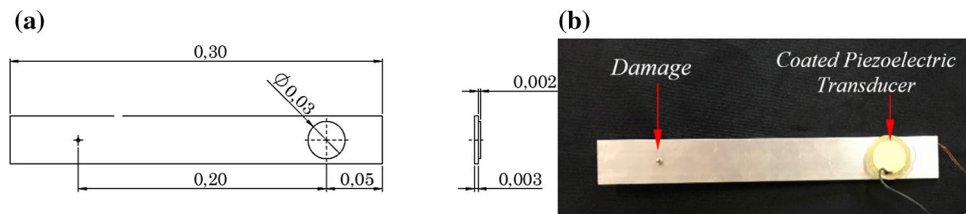


**Fig. 4** Fabrication of the coated piezoelectric transducer: **a** mold, **b** epoxy resin and sensor in the curing process, **c** coated piezoelectric transducer

**Fig. 5** Aluminum beam: **a** geometry, **b** specimen with the coated piezoelectric transducer



## 5.2 Aluminum beam

A proof-of-concept experiment was designed to evaluate the effectiveness of a piezoelectric transducer coated with epoxy to detect damage through the electromechanical impedance method. For this aim, this protected transducer was bonded on the surface of an aluminum beam ( $300 \times 38 \times 3 \text{ mm}^3$ ), as shown by Fig. 5a. A fixed bolt was removed from the beam (distant 185 mm from the piezoelectric transducer) to simulate the damage, as shown in Fig. 5b. The specimen was properly positioned inside an environmental test chamber (see Fig. 6a) to control the temperature during the acquisition of the impedance signatures. Three different temperatures were considered, namely 15 °C, 25 °C, and 35 °C. A frequency range from 40 to 70 kHz with 3.000 frequency resolution points was used in the tests. The 40–70 kHz band was determined experimentally from the analysis of the peak density in this region by performing a trial-and-error procedure, looking for the ranges that correspond to the highest peak densities since this characteristic is associated with better electromechanical coupling [11].

An in-house portable impedance meter, SySHM impedance meter [44, 45] (see Fig. 6b), was used to measure the impedance signatures before and after the damage existence.

Figure 7 shows the impedance signatures corresponding to the pristine condition for three different temperatures (15 °C, 25 °C, and 35 °C). As expected, the impedance signatures changed according to the environmental temperature [39]. This behavior can be associated with changes in the parameters of the PZT transducer [see Eq. (1)] and the

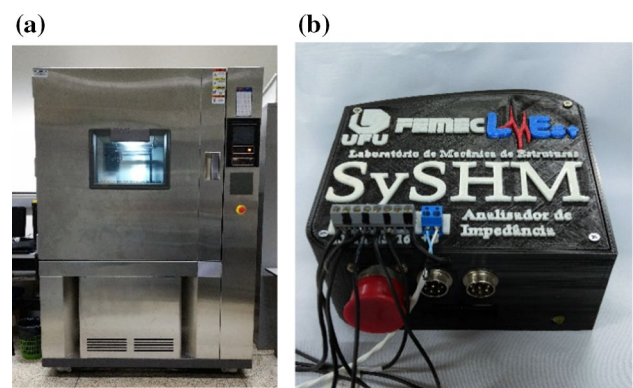


**Fig. 6** **a** Environmental test chamber, **b** portable impedance meter device

properties of the material used in the coated piezoelectric transducer.

Figures 8a, 9a, and 10a show the impedance signatures obtained at 15 °C, 25 °C, and 35 °C by using the coated piezoelectric transducer. The healthy and damaged conditions of the aluminum beam presented in Fig. 4 were considered. It is clearly visible that the impedance signatures changed with the existence of damage for the three evaluated temperatures.

Figures 9b, 10b, and 11b show the uncompensated RMSD values (compensation OFF), compensated RMSD values (compensation ON), and the thresholds obtained at 15 °C, 25 °C, and 35 °C. It is important to point out that 60 impedance measurements were performed for each temperature. The first 30 signatures were acquired for the healthy structure (pristine condition), and the remaining measurements

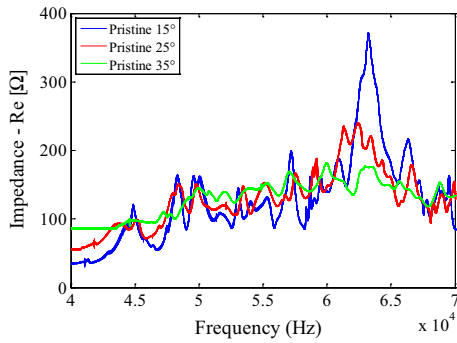


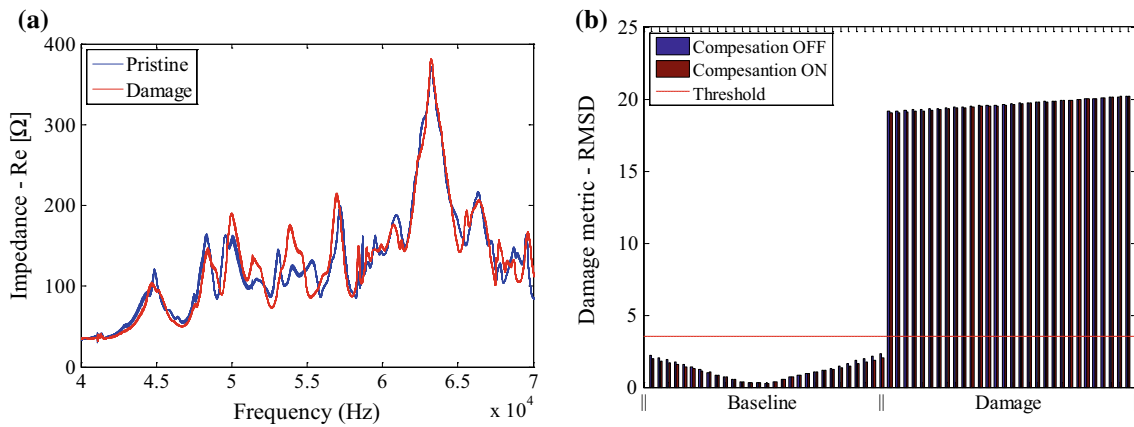
**Fig. 7** Aluminum beam with the coated piezoelectric transducer: impedance signal (pristine condition) for the three temperatures considered

were taken from the damaged beam. Note that the impedance signatures were clearly modified due to the damage existence. The RMSD damage metric was used to quantify

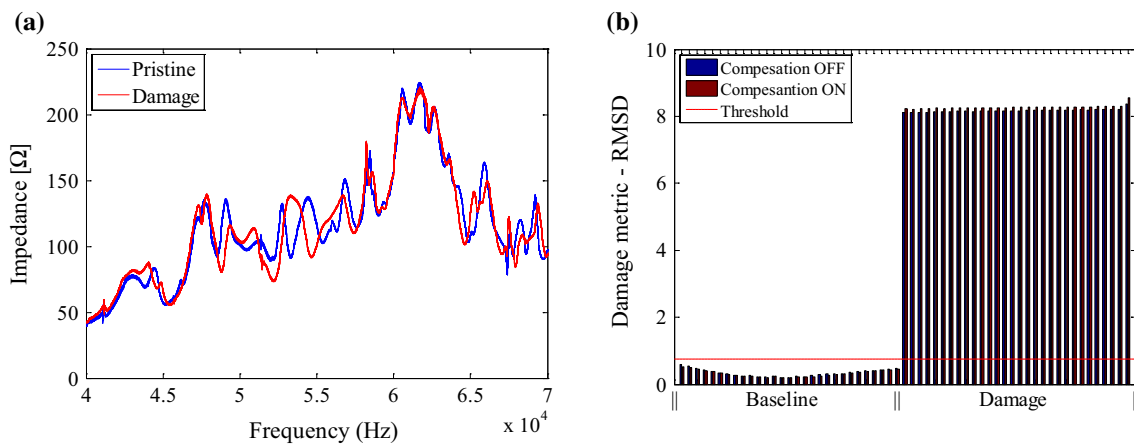
this modification, confirming the damage existence. The applied threshold value guaranteed 99% confidence regarding the probability of detection.

Figure 11a–c shows an unprotected piezoelectric transducer connected to an aluminum beam, the impedance response, and the damage metrics obtained at 15 °C, respectively. By comparing the impedance signal and the RMSD values obtained using the PZT adhesive with and without coating protection (see Figs. 8a, b, e, 11a, b), one can verify the repeatability of the tests.

This result indicates that the sensitivity of the piezoelectric transducer coated with epoxy decreases when the protection is used. However, even with lower sensitivity, the epoxy-coated sensor was able to detect incipient damage in the structure. From these previous results, it was possible to conclude that the PZT transducer coated with epoxy is effective for impedance measurements. Then, the technique



**Fig. 8** Aluminum beam with the coated piezoelectric transducer, 15 °C: **a** impedance signal, **b** compensated damage metric RMSD and the threshold value



**Fig. 9** Aluminum beam with the coated piezoelectric transducer, 25 °C: **a** impedance signal, **b** compensated damage metric RMSD and the threshold value



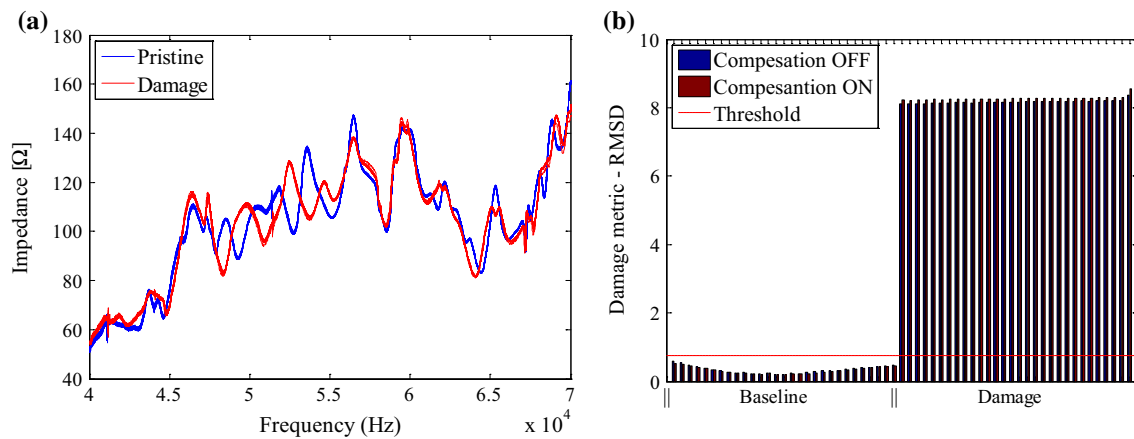
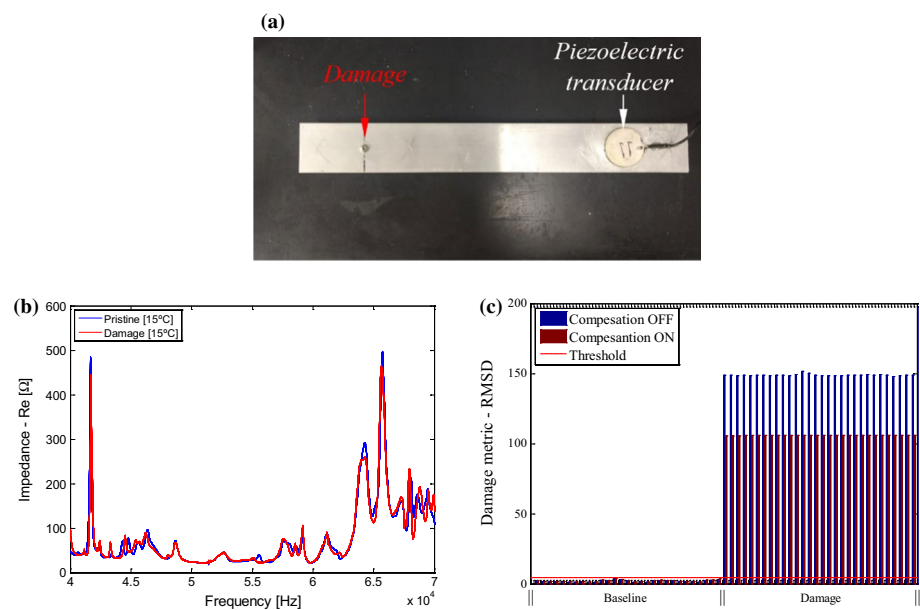


**Fig. 10** Aluminum beam with the coated piezoelectric transducer, 35 °C: **a** impedance signal, **b** compensated damage metric RMSD and the threshold value

**Fig. 11** Piezoelectric transducer attached to the aluminum beam: **a** specimen, **b** impedance signal, **c** damage metric RMSD



was ready to be tested on concrete specimens, as described in the following section.

### 5.3 Concrete specimen

In this work, the tested specimen was made of fiber-reinforced concrete, which is frequently used in recent civil engineering constructions. The material is composed of cementitious matrix reinforced with steel fibers. It is worth mentioning that the number of publications dedicated to the application of the proposed methodology to this type of composite is low, which contributes to making this contribution innovative in the area of dynamics of mechanical systems.

This composite material was made with Portland cement concrete (cement paste, aggregates, and water) and steel fibers. The steel fibers were distributed throughout the volume of the material, generating a more rigid and resistant composite. A concrete specimen was used in the tests (prismatic shape). For each case, two coated piezoceramics were embedded into the specimen. Details on the characteristics and properties of the material used can be found in [43].

A 40 MPa compressive strength ( $f_{ck}$ ) was obtained after 28 days of hydration process of the specimen. After molding, densification, and finishing, the prismatic specimen was placed inside a humid chamber for 48 h. The samples were then removed from the molds and placed under submerged curing process along 37 days.

### 5.3.1 Prismatic concrete specimen

In this context, a coated piezoelectric transducer was tested for ISHM purposes in the prismatic concrete specimen ( $500 \times 150 \times 150$  mm), as shown in Fig. 12a. Two coated piezoelectric transducers were embedded into the prismatic concrete specimen. The approximate positions of the transducers are depicted in Fig. 12b.

This experiment was performed according to two independent stages. First, the monitoring of structural integrity was made by measuring impedance signals before and after the generation of damage in the prismatic specimen. The influence of temperature was included at this stage. Later, the monitoring was performed during the test that generated the damage.

For the evaluation of the temperature effect, the specimen was properly positioned inside a thermal chamber, as previously described. In this case, 2000 frequency points resolution were acquired using the SySHM impedance meter. A frequency band of 30–80 kHz was determined experimentally for this case, for which a significant density of peaks was observed on the impedance response.

For each condition, the impedance signatures were acquired 30 times. The tests were performed for the following environmental temperatures: 10 °C, 25 °C, and 40°C. The damage was introduced in the prismatic concrete specimens through a flexural toughness test as based on the [46]. A MTS Hydraulic Servo Bending Machine was used to apply the required effort, for which the yoke device was used (see Fig. 13). The tested structure in the chamber can be observed in Fig. 14.

The impedance signatures obtained from PZT#1 (see Figs. 15a, 16a, 17a) for both the healthy and damaged prismatic specimens are presented in these figures, in which the responses measured at three different temperatures are shown. Note that the real part of the impedance signal measured for the damaged condition changed significantly as compared with the baselines (pristine conditions for the three temperatures considered).

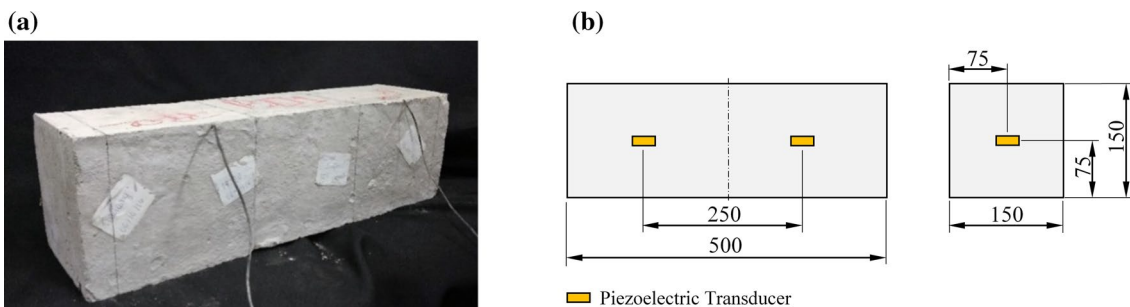


**Fig. 12** Prismatic specimen: **a** concrete specimen with coated piezoelectric transducer embedded, **b** scheme showing the positions of the transducers

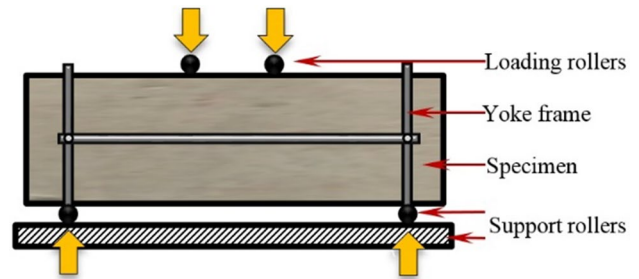


**Fig. 13** Schematic representation of the test as based on the ASTM method C1609

The damage metrics were used to quantify these changes in the impedance signatures. Similar results were found by using the damage metrics RMSD and CCD. Figures 15b, 16b, and 17b show the RMSD damage metric obtained for the thermal chamber temperature fixed at 10 °C, 25 °C, and 40 °C, respectively. Note that false positive cases were obtained due to variation in the environmental temperature. However, the compensation method was able to eliminate the false positive cases.

The first 30 measures refer to the baseline, and the other 30 are associated with the damaged condition. Note that the damage was successfully identified. The threshold was determined guaranteeing 99% confidence for the probability of detecting damage. A similar behavior was found by using the PZT#2. Once again, the temperature compensation was efficient, thus avoiding neither false positives nor false negatives during the monitoring diagnosis.

As specified earlier in this section, the second step of the experiment consisted of measuring the E/M impedance signals during the flexural toughness test, which generated damages in the studied structure. Figure 18 shows the specimen on the MTS test machine. One can see the load application system and the impedance meter SySHM connected to the piezoelectric transducers.

To avoid tearing the fibers and a possible collapse of the structure, the test was stopped as the deflection of the

**Fig. 14** **a** Prismatic specimen inside the climatic chamber, **b** detail of damage

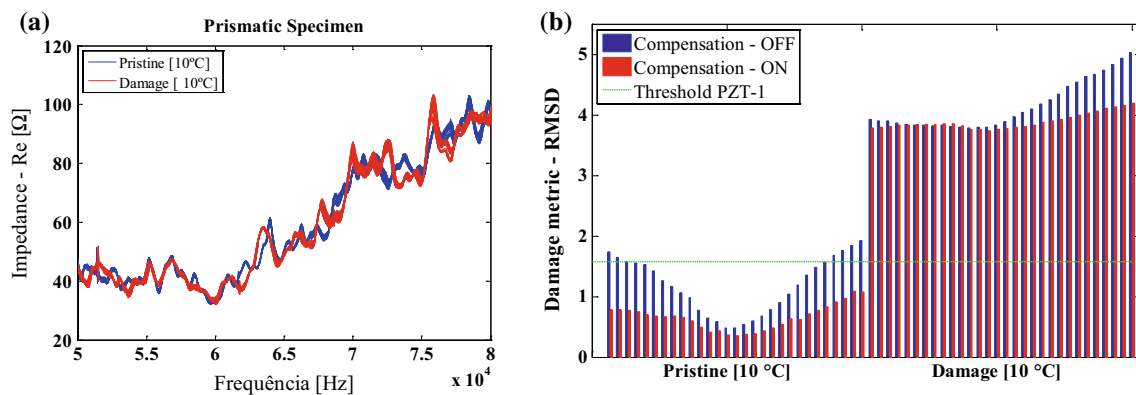
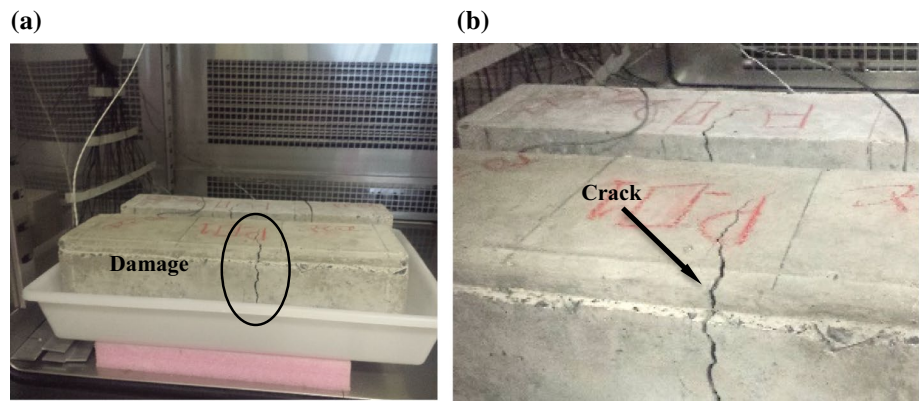


**Fig. 15** Prismatic specimen with the coated piezoelectric transducer (PZT#1/10 °C): **a** impedance signal, **b** compensated damage metric RMSD and threshold value

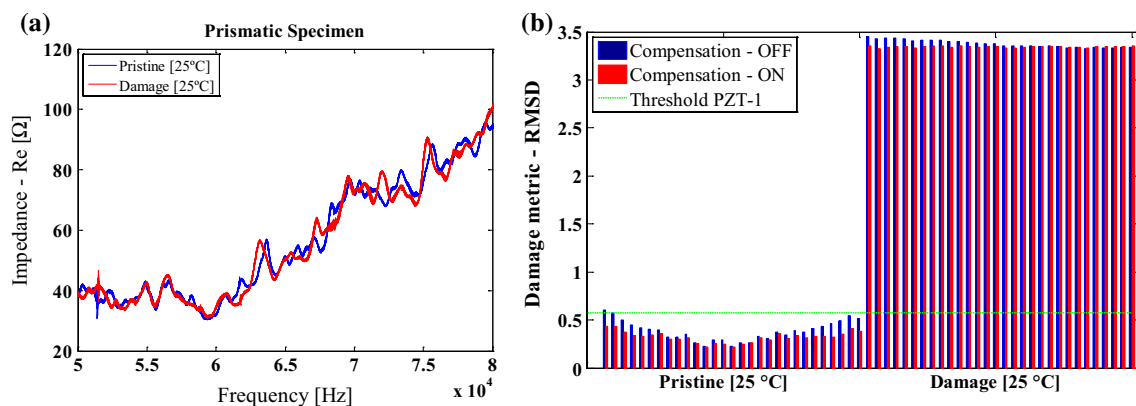


**Fig. 16** Prismatic specimen with the coated piezoelectric transducer (PZT#1/25 °C): **a** impedance signal, **b** compensated damage metric RMSD and threshold value

structure reached approximately 2.0 mm. In addition to ensuring the safety and integrity of the test machine, the propagation of cracks in the center of the specimen was considered as being sufficient for the monitoring. The load peak of approximately 54 kN, seen in Fig. 19, indicates the instant for which the structure collapses and thereafter the

load decreases and, as a result, the tenacity of the structure decreases. The role of the steel fibers in the concrete matrix is associated with the increase in the deformation due to the ability of the fibers to cross the cracks and to work as transfer bridges between the edges of the cracks, thus increasing

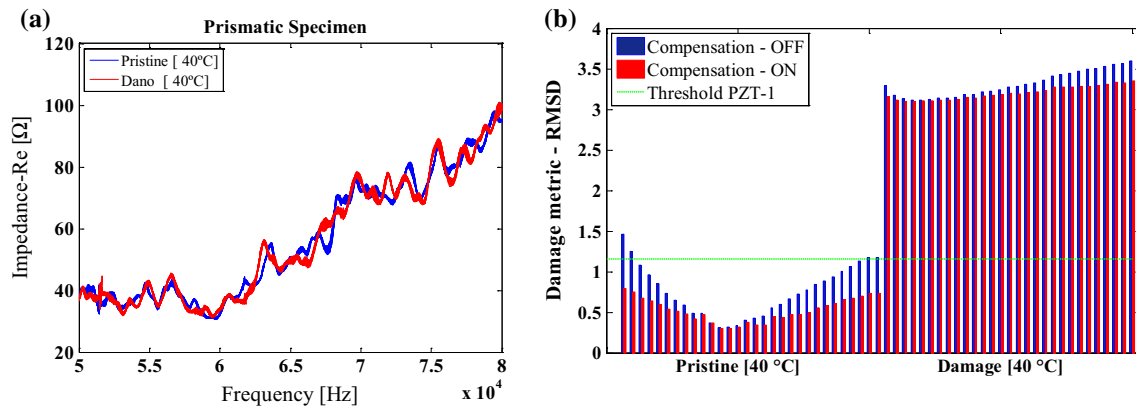


**Fig. 17** Prismatic specimen with the coated piezoelectric transducer (PZT#1/40 °C): **a** impedance signal, **b** compensated damage metric RMSD and threshold value

**Fig. 18** Specimen positioned on the MTS test machine during the flexural toughness test and the SySHM impedance meter connected to the transducers

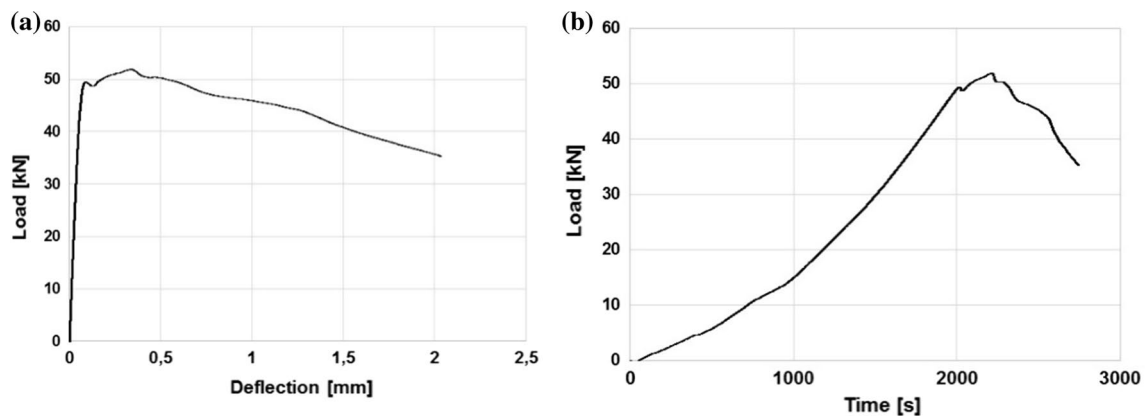
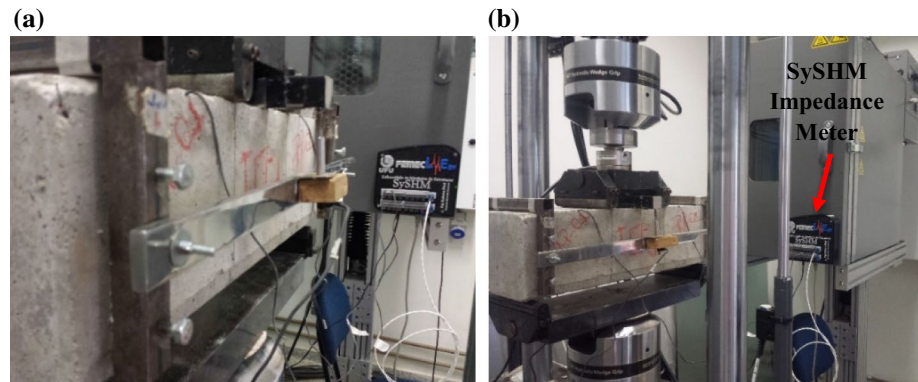


**Fig. 19** Standard ASTM C1609 test: **a** load versus deflection for a strain-softening behavior, **b** load versus time

the load capacity after the first crack. The total test time in this case was approximately 45 min.

The SySHM impedance meter was properly configured, and before starting the test, four measurements were

performed for characterizing the reference signal (baseline). Then, 48 measurements were performed during the test, i.e., the measurements were made during the loading of the structure. Finally, nine measurements were made

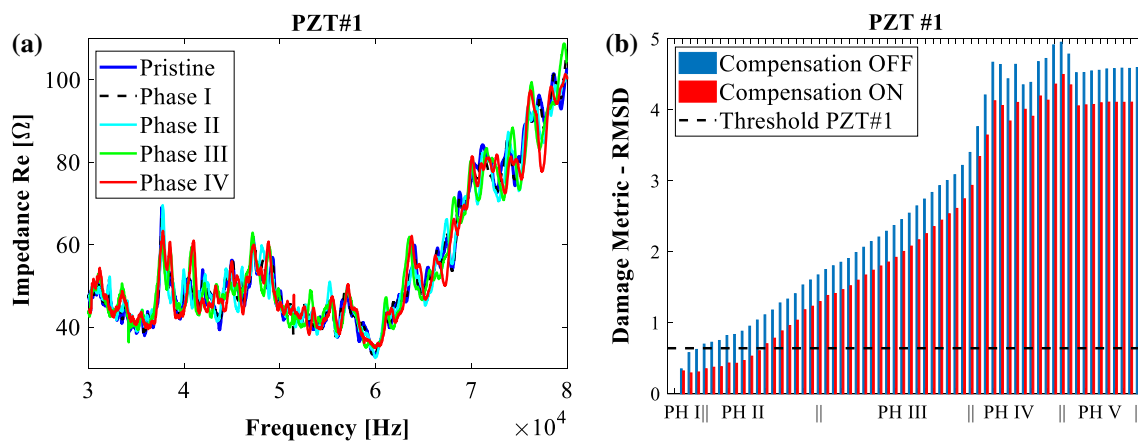


**Fig. 20** Coated piezoelectric transducer, PZT#1: **a** impedance signatures for real-time monitoring of the concrete prismatic specimen, **b** damage metric RMSD

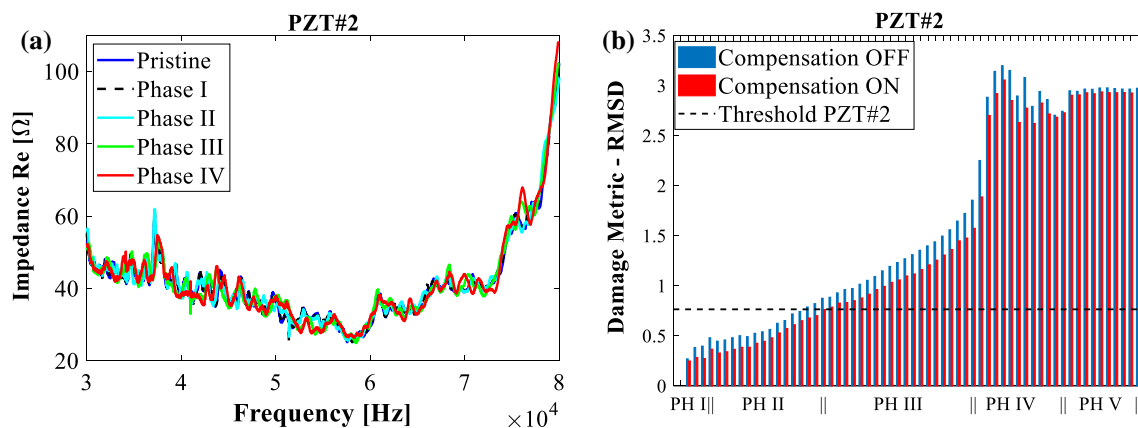


**Fig. 21** Coated piezoelectric transducer, PZT#2: **a** impedance signatures for real-time monitoring of the concrete prismatic specimen, **b** damage metric RMSD

after the end of the test, totaling 61 measures. Figures 20 and 21 show the impedance signals and the damage metric RMSD for the five different configurations of the sensors PZT#1 and PZT#2.

- PH I (Phase I): Reference signal adopted (healthy structure).
- PH II (Phase II): Initiation of the test, from the fifth to the 20th measurement. Possibly, the formation of multiple cracks occurred in this phase; the increase in the tenacity of the structure was started.
- PH III (Phase III): During this part of the test (from the 21st to the 40th measurement), the test reached the load peak (54 kN), resulting in the rupture and the maximum tenacity of the structure.
- PH IV (Phase IV): During this phase (from the 41st to 52nd measurement), after the matrix rupture, the load

capacity of the concrete does not decrease very rapidly and presents considerable tenacity.

- PH V (Phase V): After the end of the test (from the 53rd to 62nd measurement), the structure is kept at the same position, however free of loading.

It is worth mentioning that the ISHM technique was able to detect the damage for part of the situation PH II and all the other situations analyzed. Note that the RMSD values obtained on Phase V (load removed) are higher than the RMSD values obtained on phase I (healthy structure), thus demonstrating that the damage was clearly detected. In addition, as the threshold value was determined, 99% confidence was granted for the probability of damage detection. In addition, it observes a metric growth as the load and consequently the damage increase (Phases II–IV). Finally, the results above are very encouraging regarding the use of the



coated piezoelectric transducer in the context of the application of the ISHM technique. Further tests are scheduled on existing civil engineering constructions.

## 6 Conclusions

This paper proposes a SHM technique dedicated to steel fiber concrete structures using coated piezoelectric transducers embedded into the specimens to detect damage. In this context, epoxy coating is used to protect PZT transducers that are incorporated into concrete structures. The main advantage of this approach is related to the possibility of obtaining a clear indication of the presence of damage in this type of civil construction structure. It was observed that the impedance signatures obtained from coated transducers are sensitive to damage and temperature variation. In addition, the temperature compensation method based on optimization was successful on compensating for the influence of temperature on the signals, thus minimizing false diagnostics in the monitoring process. Other studies are under development aiming at other types of concrete structures, particularly on civil engineering constructions. In this case, continuous online monitoring is required. The addition of a wireless technology combined with the technique conveyed in this paper has the potential for performing remote continuous monitoring of large concrete structures.

Therefore, the main contribution of this work was to evaluate the ISHM technique using the epoxy-coated piezoelectric transducer as a sensor and actuator incorporated in a concrete sample to detect damage during the progression of structural damage. In addition, the behavior of the impedance signature was evaluated for the scenario where temperature is changing. Consequently, by analyzing the results obtained in the present study, it was possible to demonstrate that incipient cracks can be reliably detected with the ISHM method in association with the proposed data normalization technique for temperature compensation, together with the technique for statistical determination of thresholds.

**Acknowledgements** The authors would like to acknowledge CNPq (Process: 170388/2017-4, 153928/2018-2, 306200/2017-1), CAPES, and FAPEMIG for the financial support to the research work reported in this paper through the INCT-EIE.

## References

- Farrar CR, Lieven NAJ (2007) Damage prognosis: the future of structural health monitoring. *Philos Trans R Soc A* 365:623–632
- Farrar CR, Lieven NAJ, Bemend MT (2005) An introduction to damage prognosis. In: Inman DJ, Farrar CR, Junior VL, Junior VS (eds) *Damage prognosis*. Wiley, Chichester UK, pp 1–12
- Ubertini F, Comanducci G, Cavalagli N (2016) Vibration-based structural health monitoring of a historic bell-tower using output-only measurements and multivariate statistical analysis. *Struct Health Monit* 15:438–457
- Dilena M, Morassi A, Perin M (2011) Dynamic identification of a reinforced concrete damaged bridge. *Mech Syst Signal Process* 25:2990–3009
- Dilena M, Limongelli MP, Morassi A (2015) Damage localization in bridges via the FRF interpolation method. *Mech Syst Signal Process* 52:162–180
- Zhou Z, Liu W, Huang Y, Wang H, He J, Huang M, Ou J (2012) Optical fiber Bragg grating sensor assembly for 3D strain monitoring and its case study in highway pavement. *Mech Syst Signal Process* 28:36–49
- Villalba S, Casas JR (2013) Application of optical fiber distributed sensing to health monitoring of concrete structures. *Mech Syst Signal Process* 39:441–451
- Park S, Ahmad S, Yun CB, Roh Y (2006) Multiple crack detection of concrete structures using impedance-based structural health monitoring techniques. *Exp Mech* 46:609–618
- Talakokula V, Bhalla S, Gupta A (2018) Monitoring early hydration of reinforced concrete structures using structural parameters identified by piezo sensors via electromechanical impedance technique. *Mech Syst Signal Process* 99:129–141
- Chalioris CE, Karayannis CG, Angeli GM, Papadopoulos NA, Favvata MJ, Providakis CP (2016) Applications of smart piezoelectric materials in a wireless admittance monitoring system (WiAMS) to structures—Tests in RC elements. *Case Stud Constr Mater* 5:1–18
- Park G, Kabeya K, Cudney HH, Inman DJ (1999) Impedance-based structural health monitoring for temperature varying applications. *JSME Int J* 42:249–258
- Liang C, Sun FP, Rogers CA (1997) Coupled electro-mechanical analysis of adaptive material systems-determination of the actuator power consumption and system energy transfer. *J Intell Mater Syst Struct* 8:335–343
- Park G, Inman DJ (2005) Impedance-based structural health monitoring. In: Inman DJ, Farrar CR, Junior VL, Junior VS (eds) *Damage prognosis*. Wiley, Chichester, UK, pp 275–292
- Na S, Lee HK (2012) A technique for improving the damage detection ability of the electro-mechanical impedance method on concrete structures. *Smart Mater Struct* 21:1–9
- Hu X, Zhu H, Wang D (2014) A study of concrete slab damage detection based on the electromechanical impedance method. *Sensors* 14:19897–19909
- Quinn W, Kelly G, Barrett J (2011) Development of an embedded wireless sensing system for the monitoring of concrete. *J Struct Health Monit* 11:381–392
- Tawie R, Lee HK (2010) Piezoelectric-based non-destructive monitoring of hydration of reinforced concrete as an indicator of bond development at the steel–concrete interface. *Cem Concr Res* 40:1697–1703
- Talakokula V, Bhalla S, Ball JR, Bowen CR, Pesce GL, Kurchania R, Bhattacharjee B, Gupta A, Paine K (2016) Diagnosis of carbonation induced corrosion initiation and progression in reinforced concrete structures using piezo-impedance transducers. *Sens Actuators A* 242:79–91
- Lim YY, Tang ZS, Smith ST (2018) Piezoelectric-based monitoring of the curing of structural adhesives: a novel experimental study. *Smart Mater Struct* 28(1):015016
- Tang ZS, Lim YY, Smith ST, Izadgoshasb I (2019) Development of analytical and numerical models for predicting the mechanical properties of structural adhesives under curing using the PZT-based wave propagation technique. *Mech Syst Signal Process* 128:172–190

21. Gupta S, Fan G, Loh KJ (2017) Noninvasive monitoring of epoxy curing. *IEEE Sens Lett* 1(5):1–4
22. Wen Y, Chen Y, Li P, Jiang D, Guo H (2007) Smart concrete with embedded piezoelectric devices: implementation and characterization. *J Intell Mater Syst Struct* 18:265–274
23. Annamdas VGM, Yang Y, Soh CK (2010) Impedance based concrete monitoring using embedded PZT sensors. *Int J Civ Struct Eng* 1:414–424
24. Dongyu X, Sourav B, Yanbing W, Shifeng H, Xin C (2015) Temperature and loading effects of embedded smart piezoelectric sensor for health monitoring of concrete structures. *Constr Build Mater* 76:187–193
25. Liu P, Wang W, Chen Y, Feng X, Miao L (2017) Concrete damage diagnosis using electromechanical impedance technique. *Constr Build Mater* 136:450–455
26. Li W, Liu T, Wang J, Zou D, Gao S (2019) Finite-element analysis of an electromechanical impedance-based corrosion sensor with experimental verification. *J Aerospace Eng* 32:1–7
27. Zhu J, Wang Y, Qing X (2019) Modified electromechanical impedance-based disbond monitoring for honeycomb sandwich composite structure. *Compos Struct* 217:175–185
28. Malinowski P, Wandowski T, Ostachowicz W (2015) The use of electromechanical impedance conductance signatures for detection of weak adhesive bonds of carbon fiber–reinforced polymer. *Struct Health Monit* 14:332–344
29. Li W, Fan S, Ho SCM, Wu J, Song G (2018) Interfacial debonding detection in fiber-reinforced polymer rebar–reinforced concrete using electro-mechanical impedance technique. *Struct Health Monit* 17:461–471
30. Lim YY, Soh CK (2013) Damage detection and characterization using EMI technique under varying axial load. *Smart Struct Syst* 11(4):349–364
31. Wang T, Wei D, Shao J, Li Y, Gangbing G (2018) Structural stress monitoring based on piezoelectric impedance shift. *J Aerospace Eng* 31:1–8
32. Naidu ASK, Soh CK (2004) Damage severity and propagation characterization with admittance signatures of piezo transducers. *J Smart Mater Struct* 13:393–403
33. Palomino LV, Moura JRV Jr., Tsuruta KM, Rade DA, Steffen V Jr. (2011) Impedance-based health monitoring and mechanical testing of structures. *Smart Struct Syst* 7:15–25
34. Grisso BL (2004) Considerations of the impedance method, wave propagation and wireless systems for structural health monitoring. 108f. Dissertation, Virginia Polytechnic Institute and State University, Virginia
35. Peairs DM (2006) High frequency modeling and experimental analysis for implementation of impedance-based structural health monitoring, Ph.D. Thesis, Virginia Polytechnic Institute and State University, Virginia, Blacksburg, Virginia, United States of America
36. Giurgiutiu V, Zagari A (2005) Damage detection in thin plates and aerospace structure with the electro-mechanical impedance method. *Struct Health Monit* 4:99–118
37. Rabelo DS, Steffen V Jr, Finzi Neto RM, Lacerda HB (2017) Impedance-based structural health monitoring and statistical method for threshold-level determination applied to 2024–T3 aluminum panels under varying temperature. *Struct Health Monit* 16:365–381
38. Baptista FG, Budoya DE, Almeida VAD, Ulson JAC (2014) An experimental study on the effect of temperature on piezoelectric sensors for impedance-based structural health monitoring. *Sensors* 14:1208–1227
39. Price KV, Storn RM, Lampinen JA (2005) Differential evolution—a practical approach to global optimization. Springer, Berlin
40. Storn R, Price K (1997) Differential evolution: a simple and efficient adaptive scheme for global optimization over continuous spaces. *J Glob Optim* 11:341–359
41. Bendat JS, Piersol AG (2000) Random data-analysis and measurement procedures. Wiley, New York
42. Yang Y, Lim YY, Soh CK (2008) Practical issues to be application of the electromechanical impedance technique in the structural health monitoring of civil structures. *Exp Smart Mater Struct* 17:1–14
43. Silva RNF (2017) Electromechanical impedance based structural health monitoring technique applied on concrete structures. 146 f. 2017. Ph.D. Thesis, Federal University of Uberlândia, Uberlândia
44. Finzi Neto RM, Steffen V Jr., Rade DA, Gallo CA, Palomino LV (2011) A low-cost electromechanical impedance-based SHM architecture for multiplexed piezoceramic actuators. *J Struct Health Monit* 10(2011):391–402
45. Martins LGA, Finzi Neto RM, Steffen V (2012) Architecture of a remote impedance-based structural health monitoring system for aircraft applications. *J Braz Soc Mech Sci Eng* 34:393–400
46. American Concrete Institute. ASTM C1609 (2012) Standard test method for flexural performance of fiber-reinforced concrete (using beam with third-point loading). Pennsylvania, 9

**Publisher's Note** Springer Nature remains neutral with regard to jurisdictional claims in published maps and institutional affiliations.